Archetypal Visual Field Analysis of Patients With Chronic Leber Hereditary Optic Neuropathy in Relation to Visual Recovery

Catarina P. Coutinho,[1,2] Ferdinando Zanchetta,[1] Michele Carbonelli,[3] Marco Battista,[4] Alice Galzignato,[2] Chiara La Morgia,[3,5] Giulia Amore,[3] Martina Romagnoli,[6] Luigi Brotto,[7] Paolo Nucci,[7] Vincenzo Parisi,[8,9] Maria Lucia Cascavilla,[4] Leonardo Caporali,[6] Francesco Bandello,[4] Alfredo A. Sadun,[10,11] Valerio Carelli,[3,6] Rita Fioresi,[1] and Piero Barboni[2,4]

[1]Department of Pharmacy and Biotechnology, University of Bologna, Bologna, Italy
[2]Studio Oculistico d'Azeglio, Bologna, Italy
[3]Department Biomedical and Neuromotor Sciences, University of Bologna, Bologna, Italy
[4]Department of Ophthalmology, University Vita-Salute, IRCCS Ospedale San Raffaele, Milan, Italy
[5]IRCCS, Istituto delle Scienze Neurologiche, UOC Clinica Neurologica, Bologna, Italy
[6]IRCCS, Istituto delle Scienze Neurologiche, Programma di Neurogenetica, Bologna, Italy
[7]Department of Clinical Science and Community Health, University of Milan, Milan, Italy
[8]G.B. Bietti Foundation IRCCS, Rome, Italy
[9]Departmental Faculty of Medicine, UniCamillus-Saint Camillus International University of Health Sciences, Rome, Italy
[10]Department of Ophthalmology, David Geffen School of Medicine at UCLA, Los Angeles, California, United States
[11]Doheny Eye Institute, Los Angeles, California, United States

Correspondence: Piero Barboni, IRCCS San Raffaele Scientific Institute, Via Olgettina, 60, Milan 20132, Italy;
p.barboni@studiodazeglio.it.

Received: February 11, 2026
Accepted: May 20, 2026
Published: July 2, 2026

Citation: Coutinho CP, Zanchetta F, Carbonelli M, et al. Archetypal visual field analysis of patients with chronic leber hereditary optic neuropathy in relation to visual recovery. *Invest Ophthalmol Vis Sci.* 2026;67(8):8.
https://doi.org/10.1167/iovs.67.8.8

Purpose. To use the machine learning algorithm archetypal analysis (AA) to characterize visual field (VF) loss patterns in patients with chronic Leber hereditary optic neuropathy (LHON) and to determine whether these VF patterns differentiate for patients who recovered visual acuity (VA).

Methods. For patients with molecularly confirmed LHON, we retrospectively collected 30-2 or 24-2 VFs (Humphrey VF analyzer) performed at least 3 years after disease onset. A total of 220 VFs (220 eyes, 117 patients) were used as input for the AA algorithm. Archetypes (ATs) and relative weights were statistically compared between VA-recovered and not-recovered groups and among primary mitochondrial DNA mutations. K-means clustering and principal component analysis enabled two-dimensional visualization of the relationship among VFs, ATs, mean deviation, and VA.

Results. The LHON-AA model consisted of seven ATs: AT1 resembled a total loss VF pattern (30%) and AT2 a normal VF (23%). Small (AT3, 15%) and large (AT4, 10%) central scotomas followed as representative patterns. AT1 was significantly more prevalent in the not-recovered group, whereas AT2 and AT3 predominated in the recovered VA group. Less severe patterns were more present for m.14484T>C/ND6 than the other primary mutations. Two-dimensional visualization highlighted the nonlinear relationship between VA and VF outcome.

Conclusions. AA is a robust method for categorizing and quantifying VF damage in patients with chronic LHON, providing novel insights into the complexity of the disease. The findings suggest that the recovery of VA and VF damage are not transposable, although not entirely independent either, and that both parameters should be considered in the comprehensive assessment of functional recovery in LHON.

Keywords: leber hereditary optic neuropathy, archetypal analysis, machine learning, visual field, visual recovery

Leber hereditary optic neuropathy (LHON) is a potentially blinding optic neuropathy usually caused by a mitochondrial DNA (mtDNA) pathogenic variant affecting complex I of the respiratory chain. Three frequent pathogenic variants at position m.3460G>A/ND1, m.11778G>A/ND4, and m.14484T>C/ND6 are responsible for more than 90% of cases, with m.11778G>A/ND4 being the most common mutation worldwide.[1–3] Penetrance is incomplete, and the exact pathogenesis is only partly understood, with conversion from asymptomatic (carriers)

to subacute phase (affected) in about 30% of patients, mostly young males; deterioration of visual acuity is rapid in one eye, usually followed by the second eye days to months later and within a year in 97% of cases.[1] Visual loss in LHON is typically central, painless, and subacute, and visual prognosis is generally poor, with visual acuity (VA) better than 20/200 in only 5% to 10% of affected patients.[4,5]

Visual field (VF) defects in the early stages of the disease typically present as a central or cecocentral scotoma due to predominant involvement of the papillomacular bundle (PMB).[6]

The scotoma on the VF usually changes over time, starting from fixation and superior-temporal and then enlarging and extending toward the nasal side and the periphery. This corresponds to the extension of retinal nerve fiber layer damage from the PMB to the superior and inferior arcades, representing the peripheral retina as the optic nerve atrophy progresses.[7,8] Although a central scotoma is the most frequently seen, other types of scotoma can also be evident at the onset of the disease.[9] Along with the deterioration in VA, VF damage continuously progresses with time and usually reaches the nadir between 3 and 6 months of disease development, corresponding to the subacute phase of LHON; this then usually remains stable after 9 months from onset.[1,10] After 15 to 18 months from onset, in the chronic phase, patients may experience some vision recovery, either following therapy or, less commonly, spontaneously. The central scotoma may evolve favorably, manifested as a reduction in its size, or alternatively, there may emerge a small island of vision (fenestration) within the affected central area, more often in the nasal sector.[11,12]

While VA is the conventional primary endpoint in LHON recovery, it primarily assesses function in the foveal region and the PMB. This makes VA an incomplete biomarker, as it fails to capture the spatial extent and regional variability of peripheral and mid-peripheral vision loss that often persists in the chronic stage. We hypothesize that assessing VF could be important for better understanding the pathophysiology and clinical course of LHON, providing a more complete assessment of optic nerve function to predict visual outcome. However, there is a complex and often nonlinear relationship between VA and VF: clinical observations frequently reveal a "functional dissociation" in LHON, and patients may achieve meaningful VA recovery through small central fenestrations while remaining profoundly impaired by dense global scotomas or, conversely, maintain stable VA despite a progressive expansion of VF defects toward the nasal and superior sectors.[13–16] Furthermore, traditional VF metrics, such as mean deviation (MD), provide a global summary of sensitivity but reduce complex spatial patterns to a single numerical value, masking the distinct topographical characteristics of the disease.

Previous works have explored the application of archetypal analysis (AA) to identify VF loss patterns characteristic of a specific disease, such as glaucoma,[17] idiopathic intracranial hypertension,[18] and optic neuritis.[19] An AA model is composed of a number of archetypes (ATs) that represent extreme or distinct VF loss patterns and together define the boundaries of the dataset's convex hull, even when the data are heterogeneous. We previously focused on dominant optic atrophy (DOA), developing an AA model with eight ATs that enabled VF's decomposition into quantifiable patterns for VF loss characterization. The model further served to explore VF loss based on DOA genotype.[20]

The present work aims to characterize the VF damage in the LHON chronic stage employing AA; investigate if AA allows us to identify possible VF loss patterns; correlate these to visual outcome measured by final VA, visual recovery, and specific genotypes; and analyze the relationship between VA and VF, using the ATs for VF interpretation.

Methods

Patients with molecularly defined mtDNA LHON pathogenic variants were retrospectively included in the study. Clinical and VF data were retrospectively extracted from the medical records of eligible patients at the San Raffaele Scientific Institute, Milan, and the IRCCS Istituto delle Scienze Neurologiche di Bologna, Bologna, Italy. The study adheres to the Declaration of Helsinki and was approved by the San Raffaele Hospital, Milan (143/INT/2020), and Bellaria Hospital, Bologna (121/2019/OSS/AUSLBO–19012), Ethic Committee. Informed consent was obtained from all participants.

Ophthalmologic phenotyping included assessment of VA, slit-lamp biomicroscopy, intraocular pressure measurement, and indirect ophthalmoscopy. VA was assessed by measuring the best-corrected visual acuity in Snellen decimals.

Exclusion criteria comprised the presence of any retinal or optic nerve disease other than LHON, as well as spherical refractive errors greater than 5 diopters (D) or cylindrical refractive errors exceeding 2 D.

Visual Fields

For patients who underwent perimetry testing at least 3 years after disease onset (chronic stage), SITA Standard 30-2 or 24-2 Humphrey visual field tests (HFA II 750–4.1, 2005; Carl Zeiss Meditec, Dublin, CA, USA) were included to ensure that individuals were in a stable visual state and not undergoing visual recovery. Only one VF per eye was collected. VF reliability criteria were confirmed (fixation loss <33%, false-negative rate <20%, and false-positive rate <20%). The VFs were exported in a DICOM format, and the total deviations (TDs) were extracted as previously described.[20]

Archetypal Analysis Implementation

We followed the same pipeline as in our previous work.[20] The Archetypal Analysis package was implemented in Python, using the TDs of the VFs as input. No normalization of the TDs was performed, as these are already normalized according to age-matched normative values.

Using the entire dataset, we performed 10-fold cross-validation (CV) to determine the optimal number of ATs. In this context, CV is the most appropriate way to test for out-of-sample robustness of the choice of the number of ATs: the same method is also used by Elze et al.,[17] who pioneered the usage of AA analysis on VF data. The explained variance (R^2 scores) was plotted as a function of the number of ATs, and the elbow criterion was applied to identify the optimal number as previously detailed.[20] Additionally, we plotted the discrete derivative of the R^2 scores and selected the point at which the curve stabilized as the optimal number of ATs. To objectively confirm the selected number of ATs, we further applied the Bayesian information criterion (BIC) following the approach of Elze et al.[17,21]

Investigative Ophthalmology & Visual Science

The AA algorithm was then fitted to the dataset using the selected number of ATs, resulting in distinct VF loss pattern ATs. Then, we represented each VF as a convex linear combination (i.e., a weighted sum) of all selected ATs. So, for each VF, the analysis assigns a proportion to each AT, indicating how strongly each AT contributes to reconstructing the original VF. These proportions sum to 1, meaning that for each VF, we outline a combination of AT proportions, which allows successful reconstruction of the original VF. Intuitively, an AT with a higher percentage proportion indicates a higher contribution of said AT to the reconstruction of a given VF. The ATs are ordered by their average contribution across all VFs in the dataset, which is represented by the mean of the computed relative weight (RW) of the given AT, normalized to 1. Note that AA determines, in an unsupervised way, once the number of ATs has been chosen, a set of ATs that can be interpreted as "archetypal" visual loss patterns, based only on VF data. The ATs can be quantitatively related to other clinical features that are not available (exogenous) to the AA model during training, as in other studies on glaucoma.[17] Accordingly, there is no "data leakage" in our subsequent analysis. Indeed, our framework is fundamentally descriptive, contrasting sharply with predictive frameworks where algorithms are trained to predict certain features or labels in a supervised setting.

The obtained ATs were matched to corresponding VF loss patterns defined and described by the Visual Field Consensus (2022)[22] and assigned to the nerve or nonnerve fiber bundle abnormalities according to the Ocular Hypertension Treatment Study (OHTS) system.[23]

Statistical Analysis

The RWs of the ATs VF decomposition were statistically compared in two cases:

1. **Recovery analysis:** Eyes were separated into two groups based on the VA outcome: recovery of VA was defined as improvement of VA from off-chart to on-chart or for on-chart patients with an improvement of two Early Treatment Diabetic Retinopathy Study lines or more.[24,25] The Mann–Whitney *U* test was performed to statistically compare if an AT loss pattern was more prevalent in one of the two groups.
2. **Primary mutation subtype analysis:** Only VFs of patients with one of the three primary mutations (m.3460G>A/ND1, m.11778G>A/ND4, and m.14484T>C/ND6) were considered and separated accordingly. In this case, the statistical comparison was performed using the Kruskal–Wallis test with Dunn's post hoc test.

Spearman correlation analyses were performed between the ATs RW, VF mean deviation (MD, dB), and the VA (logMAR). Correlation coefficients are displayed in a heatmap, with asterisks indicating statistically significant correlations.

A significance level of 5% was considered ($P < 0.05$).

Cluster Analysis and Visualization

To visually analyze the relationship between the VF TDs (input of the AA model), the ATs (output of the AA model), the MD (VF's intrinsic parameter), and the VA (parameter that defines visual recovery), we performed the following:

1. **K-means clustering analysis:** VF TDs were partitioned into k clusters based on similarity by minimizing within-cluster variance. The optimal number of clusters was determined using the elbow criterion,[26] with the knee point automatically identified using the KneeLocator.[27] This point is defined as the location of maximum curvature, beyond which further increases yield diminishing reductions in within-cluster variance. This choice was further supported by visual inspection of the total variance as a function of the number of clusters. It should be noted that in this work, only K-means clustering was performed to simplify visual interpretation of the data distribution in the principal component analysis (PCA) space and not to define intrinsic data grouping.
2. **Visualization:** PCA was used to reduce the dimensionality of VF TDs from 54 to 2 dimensions. The same transformation was applied to the ATs to enable their representation in the same reduced space.[28] For visualization purposes, the PCA was overlaid with the K-means cluster partition defined in (1), providing a visual partition of the VF TD distribution. The VF TDs were further labeled according to the following:
   a. The MD: a quantile-based function in Python (pandas qcut) was used to define four MD intervals: better than −9 dB, between −9 and −20 dB, between −20 and −29 dB, and worse than −29 dB.
   b. If the VF corresponded to a VA-defined recovered/not-recovered case.
   c. The VA: below or equal to 0.3 logMAR to represent a recovered case with a good VA, between 0.3 and 1.0 logMAR for intermediate/borderline recovered cases, between 1.0 and 1.3 logMAR for borderline not-recovered cases, and above 1.3 logMAR representing not-recovered cases with off-chart VA.

Results

A total of 220 VFs were collected from 117 patients (220 eyes) in the chronic phase. Table 1 summarizes the characteristics of the study population, grouped by VA recovery status, along with the distribution of LHON primary mtDNA mutations.

LHON-AA Model

According to the elbow criterion, we considered 7 the optimal number of ATs (Fig. 1A) since, from this number, the R^2 scores appeared to stabilize afterward. Also, from the discrete derivative plot (Fig. 1B), a marked decrease can be

Table 1. Demographic Description of the Study Population

Characteristic	Value
Male/Female, *n*	98/19
Right/left eyes, *n*	112/108
Eyes with VA recovered/not recovered, *n*	103/117
Visual field tests (number of patients)	220 (117)
Age at examination, mean ± SD (years)	37.4 ± 18.6
Primary mutations, *n* (%)	
m.3460G>A/ND1	26 (12)
m.11778G>A/ND4	122 (55)
m.14484T>C/ND6	28 (13)
Other mtDNA mutations, *n* (%)	44 (20)

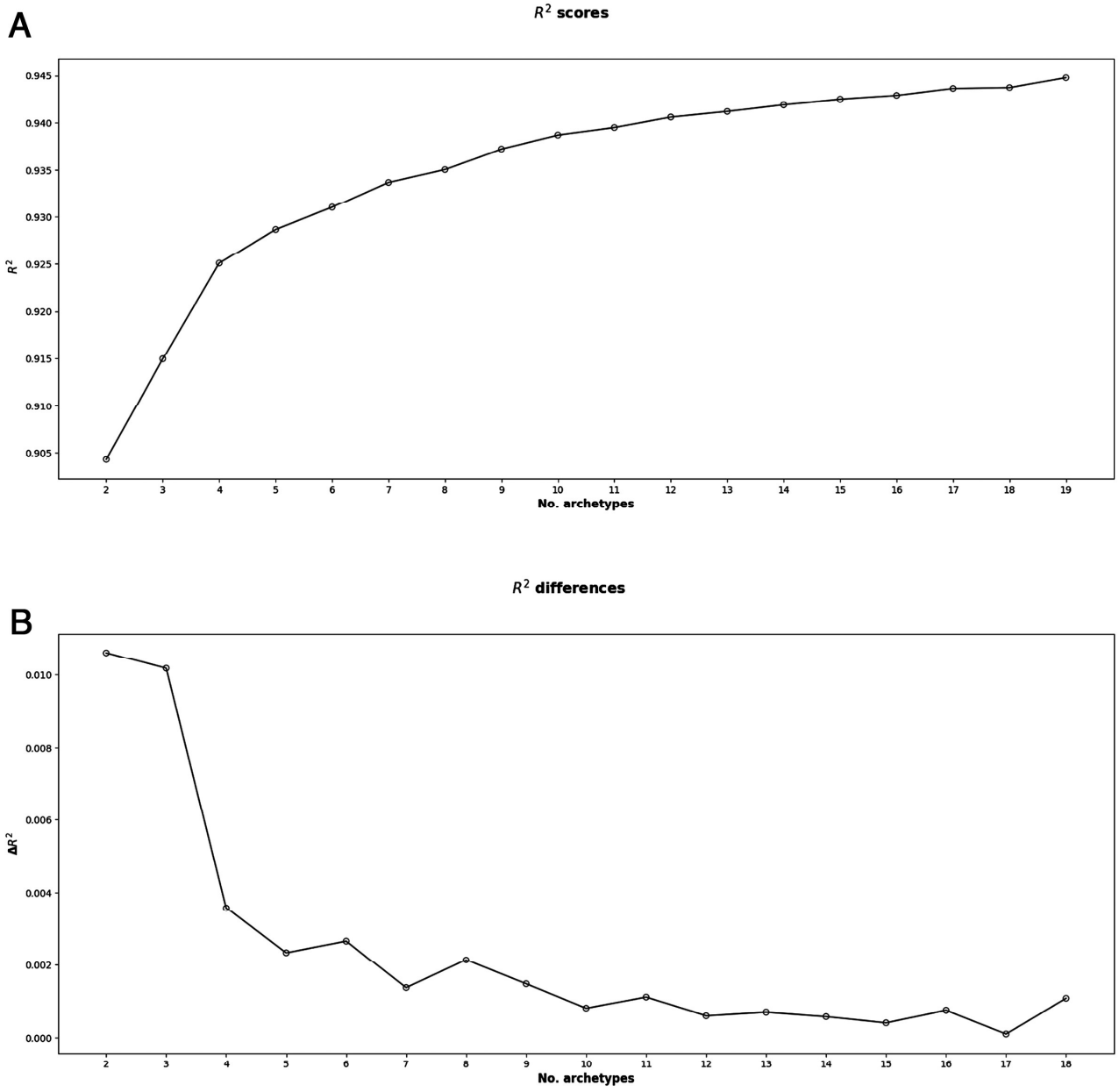

Figure 1. (**A**) Explained variance (R^2 scores) against the number of archetypes. (**B**) Discrete derivative change (ΔR^2) as a function of the difference in the number of archetypes.

depicted up to 5, followed by a further marked drop of ΔR^2 at 7, which corroborates our choice of seven ATs. In line with these observations, the BIC further confirmed our choice of the ideal number of archetypes (Supplementary Fig. A).

The developed LHON-AA model is depicted in Figure 2, with an associated R^2 score of 0.934 in 10-fold cross-validation and 0.954 in the training phase using the whole dataset. The seven ATs are ranked by their RW percentage.

Interestingly, the most prevalent ATs represent opposite VF patterns: *AT1* represents the total loss, whereas *AT2* represents a normal VF. Following the Visual Field Consensus, *AT1* and *AT6* are considered diffuse abnormalities (38%), while *AT3* and *AT4* represent central abnormalities, namely, small and large central scotomas (25%). *AT5* can be classified as a neurologic abnormality (9%) and *AT7* as a nerve fiber bundle abnormality (6%).

Regarding the OHTS system, *AT7* is related to a nerve fiber bundle defect (6%), whereas all other AT loss patterns are not related to nerve fiber bundle defects (94%).

A strong negative Spearman's correlation was found between the RW of *AT1* and VF MD (Fig. 3), meaning that an increase in the RW of the total loss AT is correlated to a decrease (worsening) of the VF MD. *AT2* and *AT3* showed a strong statistically significant positive correlation with the MD ($P < 0.001$). When correlated with VA, opposite-signed correlations were found with the same ATs: a positive correlation between *AT1* RW and VA, as well as negative correlations between *AT2* and *AT3* RWs and VA, indicating that

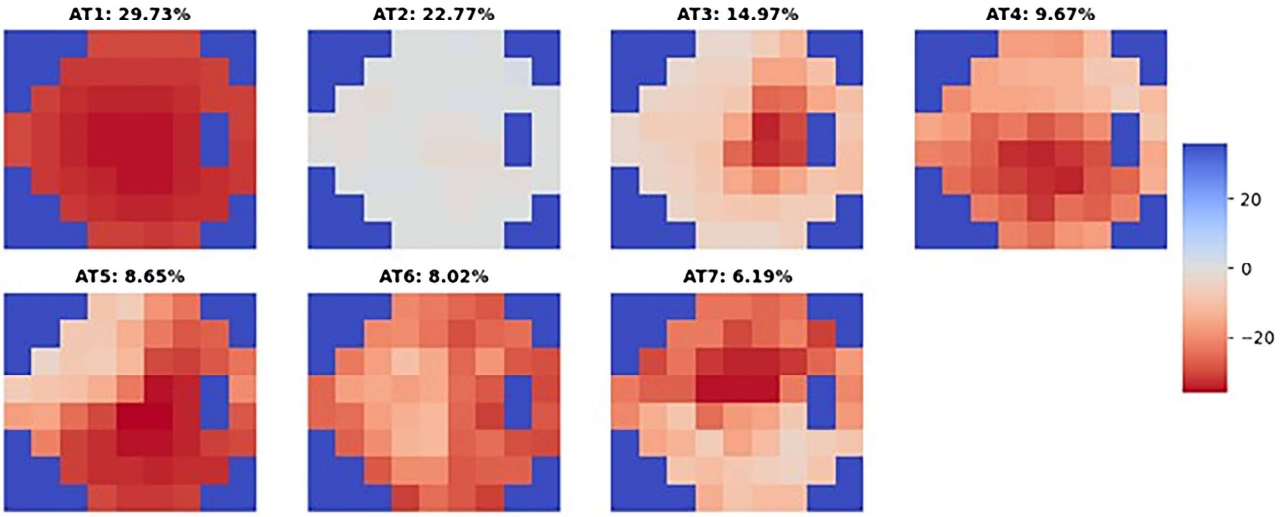

Figure 2. Obtained archetypes ordered by relative weights in percentage. *Red* represents a visual field defect with total deviations below the normal value; *dark blue* represents the blind spot and points outside the visual field test.

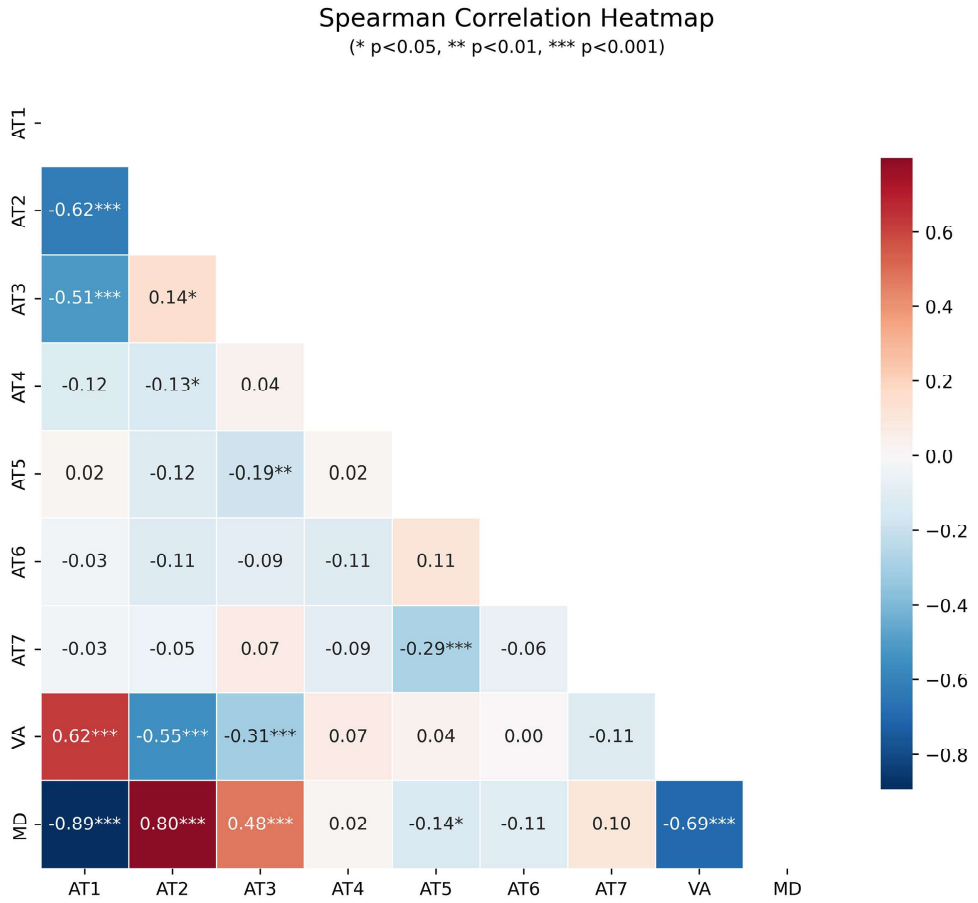

Figure 3. Spearman correlation heatmap between archetypes' weight, visual field mean deviation (in dB), and visual acuity (in logMAR). Statistical significance of 5% is represented by *, 1% by **, and 0.1% by ***.

Investigative Ophthalmology & Visual Science

Table 2. Archetypes' Relative Weight Separated Into Visual Acuity-Based Recovered and Not-Recovered Groups and Statistical Comparison Between Groups

AT	Description	Recovered (n = 103 VFs)	Not Recovered (n = 117 VFs)	P Value
AT1	Total loss	8.14	48.90	**<0.001**
AT2	Normal	39.96	7.51	**<0.001**
AT3	Small cecocentral scotoma	21.13	9.49	**<0.001**
AT4	Large cecocentral scotoma	7.49	11.61	0.271
AT5	Three quadrants	6.90	10.21	0.914
AT6	Diffuse abnormality	9.94	6.31	0.796
AT7	Altitudinal	6.43	5.97	0.353

The statistically significant correlations are highlighted in bold.

Table 3. Primary Mutation Subgroup Archetype's Relative Weight Statistical Comparison, With Global P Value and Post-Hoc Test P Values

AT	Description	A: 11778 (n = 127 VFs)	B: 14484 (n = 30 VFs)	C: 3460 (n = 30 VFs)	P Value	Post Hoc Test P Value		
						A vs. B	A vs. C	B vs. C
—	% Recovered cases	37.80	66.67	33.33	—	—	—	—
AT1	Total loss	35.99	18.95	35.68	0.116	0.147	0.790	0.158
AT2	Normal	18.28	30.13	22.49	0.202	0.254	0.853	0.853
AT3	Small cecocentral scotoma	12.68	**19.46**	13.20	**0.028**	**0.023**	0.607	0.180
AT4	Large cecocentral scotoma	10.28	**16.83**	7.90	0.068	0.105	0.382	0.081
AT5	Three quadrants	7.04	7.10	8.16	0.887	1.0	1.0	1.0
AT6	Diffuse abnormality	8.36	4.18	7.58	**0.044**	**0.048**	0.844	0.082
AT7	Altitudinal	7.36	3.35	4.98	0.229	0.346	0.637	0.346

For simplicity, m.11778G>A/ND4 is presented as 11778, m.14484T>C/ND6 as 14484, and m.3460G>A/ND1 as 3460. The statistically significant correlations are highlighted in bold.

VA (in logMAR) improved with increased RW for these ATs. Negative correlations were found between *AT1* and *AT2* and *AT1* and *AT3*, indicating that with a higher presence of the total loss archetype, there is a decrease in the normal VF resembling archetype and the central scotoma archetype.

Visual Acuity–Based Recovery Analysis

When separating VFs according to VA recovery, from the 220 VFs, 103 were considered recovered, whereas 117 were considered not recovered. High accuracy values were found when employing the LHON-AA model for both recovered (R^2 = 0.895) and not-recovered (R^2 = 0.974) groups. The VF decomposition into ATs revealed a statistically significantly higher contribution of the total loss pattern (*AT1*) in the not-recovered group (49%) compared to the recovered group (8%) (Table 2). The opposite was found for the AT, resembling a normal VF (*AT2*) that was more present in the recovered group (40%) than the not-recovered group (7%). Moreover, the small cecocentral scotomas (*AT3*) were more commonly found in the recovered group (21% vs. 9%), and this was statistically significant.

Statistically significant negative Spearman correlations were found between the RWs of *AT1*, *AT4*, *AT5*, and *AT6* and the MD for the recovered group (Supplementary Table S1). On the other hand, an increase in the RW of the normal VF resembling AT (*AT2*) was associated with an improvement in the MD (Spearman coefficient = 0.930, $P < 0.001$). Similarly, a negative correlation was found between *AT2* and VA in logMAR (Spearman coefficient = −0.252, $P < 0.001$).

For the not-recovered group, a correlation was found between the RW of the total loss AT (*AT1*) and the MD (Spearman coefficient = −0.961, $P < 0.001$), while positive correlations were found regarding *AT2*, *AT3*, *AT4*, and *AT7* (Supplementary Table S2). VA correlated positively with *AT1* (Spearman coefficient = 0.577, $P < 0.001$), whereas it correlated negatively with the small cecocentral scotoma (*AT3*; Spearman coefficient = −0.392, $P < 0.001$) and the altitudinal defect (*AT7;* Spearman coefficient = −0.258, $P = 0.005$).

Primary Mutation Subtype Analysis

In Table 3, the statistical comparison of the AT RWs is presented for the 187 VF cases with one of three primary mtDNA mutations. The application of the LHON-AA model for the VF decomposition of the three subgroups yielded high R^2 scores: 0.961 for the m.3460G>A/ND1 subgroup, 0.963 for the m.11778G>A/ND4 subgroup, and 0.924 for the m.14484T>C/ND6 cases.

A statistically significantly higher RW of *AT3* in the VF decomposition of the m.14484T>C/ND6 subgroup compared to the m.11778G>A/ND4 subgroup (P = 0.023) was found. Although not statistically significant, the total loss *AT1* was more prevalent in the m.11778G>A/ND4 (36%) and m.3460G>A/ND1 (36%) subgroups than in the m.14484T>C/ND6 (19%) subgroup. On the contrary, the normal VF pattern represented by *AT2* contributed more to the latter (30%). This is in line with the lower percentages of recovered cases in the m.11778G>A/ND4 (36%) and m.3460G>A/ND1 (36%) subgroups compared with the highest recovery percentage for the m.14484T>C/ND6 mutation (67%) subgroup.

Visual Acuity Versus Visual Field Archetypes

We explored which and how the LHON ATs obtained explain the VFs in the dataset and then distinguished the VFs according to standard clinical metrics (MD and VA). We used K-

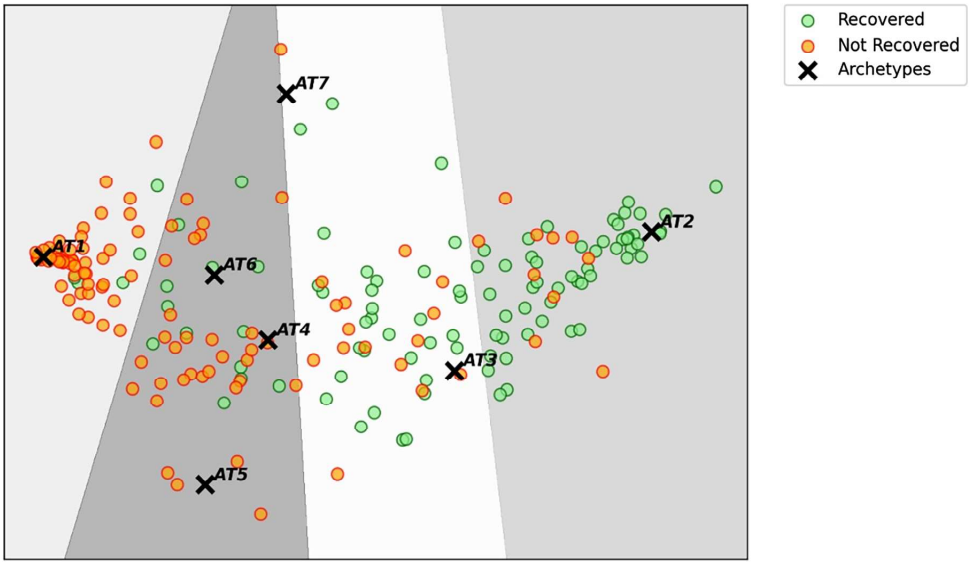

Figure 4. LHON archetype special distribution, visual field total deviation clustering, and recovery classification according to visual acuity. Visual fields K-means four clusters are represented by the different *gray colors*; *orange* visual field points represent nonrecovery visual acuity cases, and *green* points represent recovered cases; *crosses* indicate the seven archetypes of the LHON archetypal analysis model.

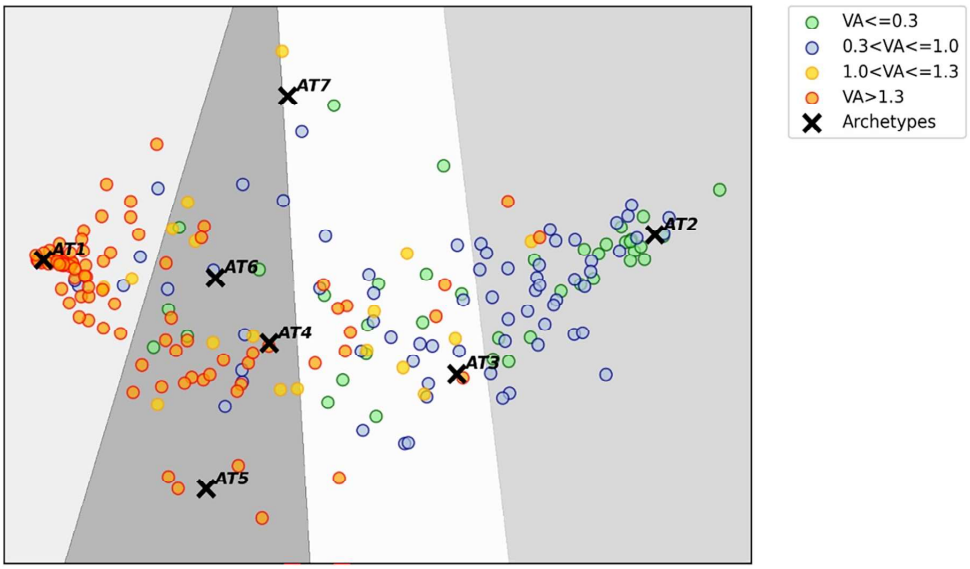

Figure 5. LHON archetype distribution for visual field total deviation clustering and visual acuity stratification. K-means four clusters are represented by the different *gray colors*; visual field *points* are stratified according to the visual acuity; *crosses* indicate the seven archetypes of the LHON archetypal analysis model.

means clustering and PCA to help us visualize these relationships.

K-means clustering of the VF TDs (k = 4, selected using the KneeLocator and the elbow criterion; Supplementary Fig. B) revealed distinct partitions of the data, shown as gray shaded areas. These clusters are meant to highlight groups of similar VFs in the plot, independently of the ATs. The data were then projected into a two-dimensional space using PCA to enable visual representation of the relationships between VF TDs, the ATs obtained, MD, and VA-based labels. In this representation, each dot corresponds to a VF, while the crosses denote the seven ATs of the LHON-AA model. The relative proximity of a VF dot to a given AT reflects its similarity to that archetypal pattern, thereby providing a visual indication of its predominant visual loss pattern.

When labeling VF dots according to the MD (Supplementary Fig. C), we showed that the VFs' clustering closely overlapped with the stratification in MD intervals (dots colored in four different colors). Furthermore, VFs with worse MD (orange dots) are close to the total loss resembling AT (*AT1*), whereas VFs with the best MD (green dots) are close to the normal VF archetype (*AT2*). VFs with an intermediate MD (yellow and blue dots) are close to different ATs, suggesting that VFs with such an MD can present different types of visual loss patterns.

Investigative Ophthalmology & Visual Science

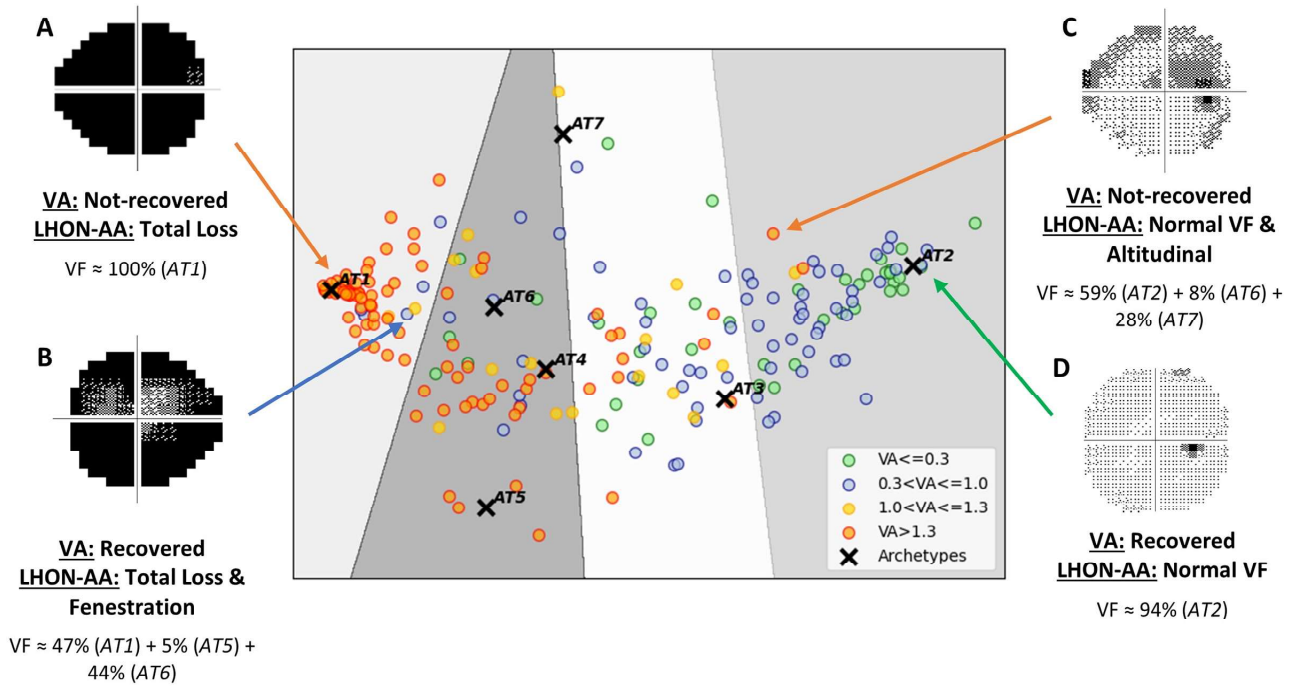

Figure 6. Examples **A–D** of visual field cases with the respective LHON archetypal analysis decomposition and label (recovered/not recovered) according to visual acuity.

Distinction of VF dots according to VA recovery or nonrecovery (Fig. 4) revealed that most of the recovered and not-recovered cases are on the two opposite clusters of the space. Furthermore, most recovered cases are close to *AT2*, the normal VF resembling AT, whereas most not-recovered cases are close to *AT1*, which represents the total loss pattern. Also, *AT3* has mostly recovered cases close by. Interestingly, these three ATs have the highest RWs in LHON-AA (Fig. 2) and were demonstrated to be statistically different between the recovered and not-recovered groups (Table 2).

When classifying VFs (dots) by VA, it is clear that AT1 is mostly associated with off-chart VA (>1.3 logMAR). Instead, *AT2* is related to a very good (≤0.3 logMAR) and intermediate VA (0.3 < VA ≤ 1.0 logMAR). However, some cases show a total loss VF (*AT1*) alongside an intermediate VA (blue dots close to *AT1* on the left side of Fig. 5). Based on VA alone, these cases would be classified as recovered despite showing extended VF damage. Similar but mirroring cases appear when a mostly good VF (*AT2* and *AT3*) comes with a low VA (orange dots close to *AT2* on the right side of Fig. 5). Therefore, we illustrate a few examples in Figure 6. In example A, which illustrates a case without VA recovery, the VF can be represented solely by the total loss pattern (*AT1*). In contrast, example B represents a case with VA recovery associated with a defect. In this case, the decomposition of the ATs shows both the total loss pattern and the presence of fenestration (*AT6*), which likely accounts for the VA recovery, as the center of the visual field defect remains relatively intact. On the right side, in example D, we see a typical normal VF of a VA recovery patient, whereas in example C, we have a non-VA recovery patient with a high percentage of normal VF but with a component of the altitudinal (*AT7*) and central scotoma (*AT3*) in the VF AT decomposition that highlights the impact of a central defect on the VA.

Discussion

In the study, the application of AA to VFs in patients with chronic LHON enabled us to characterize patterns of VF damage at this stage of the disease and to identify seven distinct ATs. This approach provided a structured framework for describing the variability of VF loss among patients. Moreover, by applying the AA model, we explored how these VF ATs relate to VA recovery (or nonrecovery). Finally, through the AA model, we established a meaningful relationship between the extent of VF damage and VA, offering new insights into how similar VA outcomes in patients with chronic LHON may actually correspond to distinct VF patterns.

In the acute stage of LHON, the central scotoma typically appears as cecocentral and then progressively enlarges in parallel to the development of optic atrophy. In the chronic stage of the disease, a variable VF defect remains, which varies from case to case, preventing us from providing a standardized interpretation.[7,8] The AA analysis allowed us to classify the final VF defect by assigning weights to the different AT patterns that make up the VF. The AA analysis led to the definition of seven representative patterns, among which, apart from the extremes (*AT1* and *AT7*), the most prevalent corresponds to cecocentral scotomas (*AT3* and *AT4*) (Fig. 2). The correlation of the results obtained between each AT and MD, as well as between each AT and VA, further strengthens the clinical understanding of the disease (Fig. 3). Notably, it has been demonstrated that the MD can accurately reflect deteriorating visual function in patients with LHON.[29]

The recovery or nonrecovery of visual function has conventionally been based on the VA; AT patterns differed between groups, with some ATs being more prevalent in one group (Table 2). Higher RWs of *AT2* and *AT3* patterns,

indicative of minor and less severe VF defects, were associated with a more favorable outcome, whereas *AT1* and *AT4* patterns, reflecting extensive scotomas, were linked to a poorer prognosis.

Notably, the most preserved sector of the VF is the nasal region, particularly the superior region, regardless of VA recovery. This finding may suggest that this sector is either the most preserved during the acute phase or the one with the greatest potential for recovery in the chronic phase, even without improvement in VA.[11] In our AA model, the temporal sectors were more often affected in *AT3*, *AT5*, and *AT6*, while nasal sectors were more consistently spared, consistent with previous clinical and histopathologic observations.[11] The recovery potential associated with this pattern has been hypothesized to be related to the asymmetric distribution of retinal ganglion cell types, with a higher density of midget and parasol cells in the temporal macular region compared to the nasal side.[30]

We analyzed the RW of individual AT patterns separately for each primary mutation; the only differences observed were related to the higher frequency of recovery in the m.14484T>C/ND6 mutation, where *AT2* and *AT3* patterns were more common, and *AT1* and *AT6* were less prevalent (Table 3). Interestingly, *AT4* appears to have a higher RW for the m.14484T>C/ND6 mutation, which may be linked to VA recovery due to fenestration of the large central scotoma; therefore, this pattern is probably characteristic of this mutation. Although not statistically significant, the observed trend toward more favorable VF outcomes in m.14484T>C cases is consistent with prior literature, in which the m.14484T>C mutation is associated with a comparatively better visual prognosis.[5] Ideally, these findings should be confirmed in a larger and more mutation-balanced sample.

To provide a clinically interpretable meaning of our AA analysis, we used PCA, which allowed us to reduce the dimensionality of each VF and project them onto a two-dimensional plot using the first two principal components. In this plot, ATs were successively added to act as reference points. The relative position of each VF with respect to the ATs reflects its composition in terms of archetypal weights, so that the proximity of a VF to a given AT indicates a stronger contribution of that AT pattern to the reconstruction of said VF.

To further facilitate visual interpretation of the data points in this reduced space, we applied K-means clustering to the total deviation values of the VFs. The resulting partitions highlight regions of relatively homogeneous data density, which should be considered visual guidance rather than approximations of the ATs. In this plot (Fig. 4), a clear separation is depicted. On one hand, VA recovery cases tend to lie closer to the normal VF AT; on the other hand, nonrecovery cases are generally placed near the AT representing total loss. However, this separation became less evident when intermediate VA levels were considered (Fig. 5). Overall, the two-dimensional plots indicate that the relationship between VA recovery and VF patterns is not one-to-one: similar VA outcomes can arise from different regions of the archetypal space, with some recovered cases showing relatively worse VF patterns and some not-recovered cases showing comparatively better VFs (examples in Fig. 6).

These findings suggest that there is no linear relationship between VA recovery and VF outcome. Future analyses of VF progression are warranted to help identify specific VF recovery patterns. In the long term, distinguishing VA from VF recovery may provide valuable insights into pathophysiology and the definition of visual prognosis in patients with LHON.

From a machine learning perspective, the application of AA to study VF defects in patients with chronic LHON demonstrated not only strong performance with high accuracy but also results that are clinically consistent with previous findings. Furthermore, our new results provided insights into the relationship between VA recovery and VF damage. Moreover, the obtained ATs were shown to lie along the perimetry enclosing the data cloud, effectively capturing the extremes of the observed variability and representing the fundamental patterns despite the heterogeneity of mutations. These findings highlight the robustness and interpretability of AA as a tool for VF data analysis.

This study has several limitations. One is the sample size, which is bound by the rarity of LHON. Indeed, while we employed cross-validation to assess the number of ATs to use for our model (the main hyperparameter that can lead an AA model to overfit the data and that needs to be tuned), following Elze et al.,[17,21] the sample size prevented us from identifying an adequate held-out test set to perform an out-of-sample evaluation of the convex hull described by our ATs. Note, however, that a test set for this purpose was not always used to assess an AA model.[17,21] As a consequence, we conducted statistical analyses of the AT weights using the same data we used to fit our AA model. As the identification of the ATs is unsupervised and independent from our statistical analyses and the computation of the AT relative weights is deterministic once the ATs have been fixed (in machine learning terminology, they are new features, not parameters learned by a supervised model), this does not give rise to what is known in machine learning as "data leakage." Nevertheless, as the generalizability to the general population of our conclusions depends on how well the convex hull determined by the ATs we found using our dataset fits the wider population's data, it is possible that some correlations we found are optimistic and do not generalize in the same way to out-of-sample data coming from another center if our AA model is used. Second, subgroup comparison of ATs' RW across primary mutations was affected by unequal group sizes. In this context, the lack of statistical significance should be interpreted carefully, as it may reflect limited statistical power rather than the absence of a clinically meaningful difference. Importantly, this imbalance reflects the known distribution of primary LHON mutations, which limits the feasibility of achieving fully balanced mutation-based groups for clinical studies. Finally, a longitudinal assessment could show if known visual field evolution is captured quantitatively by using the ATs we identified. This will be the subject of future work.

The evaluation of VF and VA during the chronic phase of LHON suggests distinct patterns of VA recovery and VF damage, highlighting the need for independent assessment. A detailed investigation of the natural history of LHON, encompassing the transition from the acute to the chronic phase in VF and VA, will be essential to elucidate the factors and mechanisms underlying this complex disease. Approaches such as the one we introduce to characterize this dichotomy may provide a more precise framework for the stratification of patients in clinical trials.

Acknowledgments

Supported by a research scholarship funded by the European Union-Next Generation EU, Missione 4 Component 1 CUP

J33C24001310009 (CPC); CaLISTA CA 21109; CaLIGOLA MSCA-2021-SE-01-101086123; MSCA-DN CaLiForNIA—101119552; PNRR MNESYS, the PNRR National Center for HPC, Big Data, and Quantum Computing CUP J33C22001170001; SimQuSec CUP J13C2200068000; INFN Sezione Bologna, Gast initiative; GNSAGA Indam (RF, FZ). CLM and VC are members of the European Reference Network for Neuromuscular Diseases (EURO-NMD).

Presented in part at the Association for Research in Vision and Ophthalmology 2024 Annual Meeting, Seattle, Washington, USA, May 5–9, 2024.

Disclosure: **C.P. Coutinho**, None; **F. Zanchetta**, None; **M. Carbonelli**, None; **M. Battista**, None; **A. Galzignato**, None; **C. La Morgia**, None; **G. Amore**, None; **M. Romagnoli**, None; **L. Brotto**, None; **P. Nucci**, None; **V. Parisi**, None; **M.L. Cascavilla**, None; **L. Caporali**, None; **F. Bandello**, None; **A.A. Sadun**, None; **V. Carelli**, None; **R. Fioresi**, None; **P. Barboni**, GenSight Biologics (C), Santhera Pharmaceuticals (R), Chiesi Farmaceutici (R), Omikron Italia (R); he is SI for clinical trials sponsored by GenSight Biologics and Santhera. None of these activities are related to conduction of this study and the writing of the manuscript

References

1. Carelli V, Carbonelli M, de Coo IF, et al. International consensus statement on the clinical and therapeutic management of Leber hereditary optic neuropathy. *J Neuroophthalmol*. 2017;37(4):371–381.
2. Yu-Wai-Man P, Votruba M, Burté F, La Morgia C, Barboni P, Carelli V. A neurodegenerative perspective on mitochondrial optic neuropathies. *Acta Neuropathol*. 2016;132(6):789–806.
3. Newman NJ, Lott MT, Wallace DC. The clinical characteristics of pedigrees of Leber's hereditary optic neuropathy with the 11778 mutation. *Am J Ophthalmol*. 1991;111(6):750–762.
4. Newman NJ, Carelli V, Taiel M, Yu-Wai-Man P. Visual outcomes in Leber hereditary optic neuropathy patients with the m.11778G>A (MTND4) mitochondrial DNA mutation. *J Neuroophthalmol*. 2020;40(4):547–557.
5. Yu-Wai-Man P, Newman NJ, Carelli V, et al.; LHON REALITY Study Group. Natural history of patients with Leber hereditary optic neuropathy—results from the REALITY study. *Eye (Lond)*. 2022;36(4):818–826.
6. Sadun AA, Win PH, Ross-Cisneros FN, Walker SO, Carelli V. Leber's hereditary optic neuropathy differentially affects smaller axons in the optic nerve. *Trans Am Ophthalmol Soc*. 2000;98:223–235.
7. Wakakura M, Fujie W, Emoto Y. Initial temporal field defect in Leber hereditary optic neuropathy. *Jpn J Ophthalmol*. 2009;53(6):603–607.
8. Newman NJ, Biousse V, Newman SA, et al. Progression of visual field defects in Leber hereditary optic neuropathy: experience of the LHON treatment trial. *Am J Ophthalmol*. 2006;141(6):1061–1067.
9. Barboni P, Sadun AA. *Atlas of LHON*. Breukelen, Netherlands: MEDonline; 2019.
10. Liu HL, Yuan JJ, Tian Z, Li X, Song L, Li B. What are the characteristics and progression of visual field defects in patients with Leber hereditary optic neuropathy: a prospective single-centre study in China. *BMJ Open*. 2019;9(3):e025307.
11. Mashima Y, Sato EA, Ohde H, Oguchi Y. Macular nerve fibers temporal to fovea may have a greater potential to recover function in patients with Leber's hereditary optic neuropathy. *Jpn J Ophthalmol*. 2002;46(6):660–667.
12. Kishi M, Ueda K, Kurimoto T, Nakamura M. Correlation between residual sensitivity in the central inferior nasal visual field and visual function in chronic Leber hereditary optic neuropathy patients. *Ophthalmic Res*. 2024;67(1):1–8.
13. Sadun AA, Salomao SR, Berezovsky A, et al. Subclinical carriers and conversions in Leber hereditary optic neuropathy: a prospective psychophysical study. *Trans Am Ophthalmol Soc*. 2006;104:51–61.
14. Stone EM, Newman NJ, Miller NR, Johns DR, Lott MT, Wallace DC. Visual recovery in patients with Leber's hereditary optic neuropathy and the 11778 mutation. *J Clin Neuroophthalmol*. 1992;12(1):10–14.
15. Nakamura M, Yamamoto M. Variable pattern of visual recovery of Leber's hereditary optic neuropathy. *Br J Ophthalmol*. 2000;84(5):534–535.
16. Yuan JJ, Zhang Y, Wang LL, et al. Visual field variability after gene therapy for Leber's hereditary optic neuropathy. *Ophthalmic Res*. 2018;60(3):176–184.
17. Elze T, Pasquale LR, Shen LQ, Chen TC, Wiggs JL, Bex PJ. Patterns of functional vision loss in glaucoma determined with archetypal analysis. *J R Soc Interface*. 2015;12(103):20141118.
18. Wang M, Shen LQ, Pasquale LR, et al. An artificial intelligence approach to detect visual field progression in glaucoma based on spatial pattern analysis. *Invest Ophthalmol Vis Sci*. 2019;60(1):365–375.
19. Solli E, Doshi H, Elze T, Pasquale L, Wall M, Kupersmith M. Archetypal analysis reveals quantifiable patterns of visual field loss in optic neuritis. *Transl Vis Sci Technol*. 2022;11(1):27.
20. Coutinho CP, Zanchetta F, Carbonelli M, et al. Machine learning applied to visual fields of dominant optic atrophy patients. *Transl Vis Sci Technol*. 2025;14(6):20.
21. Gazanchian M, Nejad A, Crabb DP, Montesano G, Jansonius NM. Archetypes of binocular visual field loss and their impact on vision-related quality of life in glaucoma patients. *Invest Ophthalmol Vis Sci*. 2026;67(3):28.
22. Kruger JM, Almer Z, Almog Y, et al. A consensus statement on the terminology for automated visual field abnormalities. *J Neuroophthalmol*. 2022;42(4):483–488.
23. Keltner JL, Johnson CA, Cello KE, et al.; Ocular Hypertension Treatment Study Group. Classification of visual field abnormalities in the ocular hypertension treatment study. *Arch Ophthalmol*. 2003;121(5):643–650.
24. Sanders FWB, Votruba M. Outcomes of idebenone therapy for Leber hereditary optic neuropathy in a cohort of patients from Wales. *Eye (Lond)*. 2025;39(16):2952–2957.
25. Klopstock T, Yu-Wai-Man P, Dimitriadis K, et al. A randomized placebo-controlled trial of idebenone in Leber's hereditary optic neuropathy. *Brain*. 2011;134(pt 9):2677–2686.
26. Thorndike RL. Who belongs in the family? *Psychometrika*. 1953;18:267–276.
27. Hastie T, Tibshirani R, Friedman JH. *The Elements of Statistical Learning: Data Mining, Inference, and Prediction*. 2nd ed. New York, USA: Springer; 2009.
28. Satopää V, Albrecht J, Irwin D, Raghavan B. Finding a "kneedle" in a haystack: detecting knee points in system behavior. In: *31st International Conference on Distributed Computing Systems Workshops*. Los Alamitos, California, USA: IEEE/IEEE Computer Society; 2011:166–171.
29. Ran R, Yang S, He H, Ma S, Chen Z, Li B. A retrospective analysis of characteristics of visual field damage in patients with Leber's hereditary optic neuropathy. *Springerplus*. 2016;5(1):843.
30. Sadun AA, Win PH, Ross-Cisneros FN, Walker SO, Carelli V. Leber's hereditary optic neuropathy differentially affects smaller axons in the optic nerve. *Trans Am Ophthalmol Soc*. 2000;98:223–235.